The Journal of Chemical Physics

ARTICLE

pubs.aip.org/aip/jcp

Investigating the ultraviolet photodissociation of bromocyclopropane with ultrafast electron diffraction

Cite as: J. Chem. Phys. **163**, 174306 (2025); doi: 10.1063/5.0293140
Submitted: 25 July 2025 • Accepted: 17 October 2025 •
Published Online: 4 November 2025

View Online Export Citation CrossMark

Jackson Lederer,[1,a)] J. Pedro F. Nunes,[2] Conor D. Rankine,[3] Andrew R. Attar,[4] Kareem Hegazy,[4] Fuhao Ji,[4] Cuong Le,[1] Ming-Fu Lin,[4] Yusong Liu,[4] Duan Luo,[4] Andrew J. Orr-Ewing,[5] Sajib Kumar Saha,[1] Xiaozhe Shen,[4] Xijie Wang,[6,7] Matthew Ware,[8] Stephen P. Weathersby,[4] Kyle J. Wilkin,[1] Thomas J. A. Wolf,[8] Yanwei Xiong,[1] Jie Yang,[9] and Martin Centurion[1,a)]

AFFILIATIONS

[1] Department of Physics and Astronomy, University of Nebraska-Lincoln, Lincoln, Nebraska 68588, USA
[2] Diamond Light Source Ltd, Diamond House, Harwell Campus, Didcot OX11 0D, United Kingdom
[3] Department of Chemistry, University of York, Heslington, York YO10 5DD, United Kingdom
[4] SLAC National Accelerator Laboratory, Menlo Park, California 94025, USA
[5] School of Chemistry, University of Bristol, Cantock's Close, Bristol BS8 1TS, United Kingdom
[6] Faculty of Physics, University of Duisburg-Essen, 47048 Duisburg, Germany
[7] Department of Physics, TU Dortmund University, 44227 Dortmund, Germany
[8] Stanford PULSE Institute, SLAC National Accelerator Laboratory, Menlo Park, California 94025, USA
[9] Department of Chemistry, Tsinghua University, Beijing 100084, People's Republic of China

[a)] **Authors to whom correspondence should be addressed:** jacksonlederer@huskers.unl.edu and martin.centurion@unl.edu

ABSTRACT

We have studied the photodissociation of gas-phase bromocyclopropane by 200 nm wavelength ultraviolet radiation using ultrafast electron diffraction. Bromocyclopropane is a prototypical molecule in the study of organobromides, a class of molecules that have a significant impact on atmospheric ozone depletion through their photochemistry. Previous studies have revealed two possible reaction pathways for the photodissociation of bromine from bromocyclopropane; either the C–Br bond dissociates, leaving behind a cyclopropyl ring, or there is a concerted opening of the cyclopropyl ring along with the C–Br bond dissociation. In this work, both our experimental and simulation results indicate that the majority of the UV-photoexcited BCP molecules (88% ± 11% in the experiment) follow the first reaction pathway, in which the cyclopropyl ring remains closed after homolytic C–Br bond cleavage. This direct bond dissociation occurs within the experimental time resolution of 270 fs. In order to differentiate between the possible reaction end-products, both of which have diffraction signals dominated by the bromine atom, a new analysis method has been employed, which is more sensitive to the structure of the end-products.

I. INTRODUCTION

Bromocyclopropane (BCP) is a prototypical molecule for the study of organobromides, a class of molecules that have a significant impact on the Earth's atmospheric ozone through their photochemistry.[1,2] In the atmosphere, organobromides photodissociate on the absorption of UV photons, producing bromine atoms and other species that catalyze reactions that break down the Earth's ozone layer.[3,4] In addition, the photofragments of organobromides have been shown to cause DNA damage, leading to a possible increase in cancer and other negative health effects.[5] In order to better understand the impacts of the photodissociation of organobromide molecules, we must first develop a mechanistic understanding of these reactions. In a previous study of BCP using velocity-map imaging,[6] two possible photodissociation pathways were proposed. In the predominant reaction pathway (pathway A in Fig. 1), the

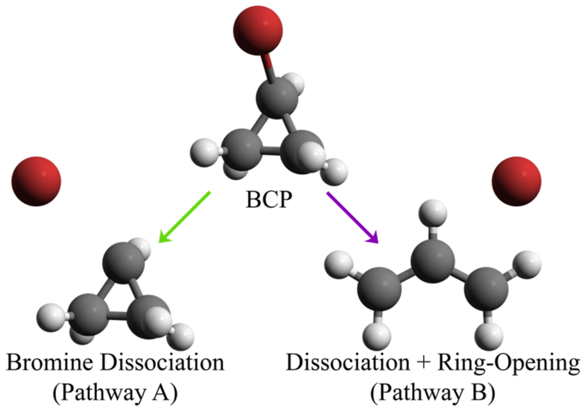

FIG. 1. Schematic showing the two possible photodissociation pathways of the BCP reaction. For BCP molecules following pathway A, the bromine photodissociation leaves behind a bromine radical and a cyclopropyl ring. In pathway B, the cyclopropyl ring opens, yielding an allyl radical following the bromine photodissociation.

homolytic fission of the bromine–carbon bond yields a cyclopropyl radical and a bromine atom. Evidence was also presented for a second, minor reaction pathway (pathway B), in which a concerted opening of the cyclopropyl ring occurs simultaneously with the dissociation of the bromine atom. Concerted ring-opening has also been observed in nanosecond studies of BCP in solution[7] and iodocyclopropane[8] in both the gas and solution phases. While allyl radicals have been seen as ring-opening reaction products at longer timescales, experiments to date have lacked the necessary spatiotemporal resolution to determine the reaction pathways at short timescales, i.e., on the order of femto- and picoseconds.

In order to follow the reaction more closely, we have carried out ultrafast electron diffraction (UED) measurements of photoexcited BCP at the SLAC National Accelerator Laboratory. Gas electron diffraction has previously been used to determine the ground-state structure of BCP.[9] UED is capable of observing changes in molecular geometries[10] during pump–probe experiments and enables measurements with both femtosecond temporal resolution and sub-angstrom spatial resolution.[11,12] The use of mega-electron volt (MeV) UED overcomes some of the drawbacks of previous electron diffraction experiments, such as the velocity mismatch between the pump and probe pulses and the broadening of the electron probe pulse due to Coulomb forces.[13,14] Together, these unique attributes have made UED an attractive and effective tool to study, e.g., the reaction dynamics of photodissociation in the gas phase,[15–19] and to explore the dynamics in ring-opening reactions.[20,21] This UED experiment uses 200 nm laser pulses to excite gas-phase BCP molecules and 3.7 MeV electrons to probe the resulting structural changes. Upon excitation at 200 nm, BCP is likely excited to one or more electronic states in the A band, previously labeled as $^3Q_1$, $^3Q_0$, and $^1Q_1$, in which a non-bonding electron in one of the orbitals on the Br atom is excited into the anti-bonding C–Br σ^* orbital.[6,22] Based on our trajectory simulations, we see no evidence of exciting to Rydberg states. From this experiment, we have determined the yield of the different reaction channels immediately after C–Br bond dissociation by comparison with simulated fragment geometries. Due to the much larger electron scattering amplitude of bromine relative to carbon and hydrogen, the time-dependent difference signal depends largely on the dissociation of bromine. Consequently, we have employed a new data analysis method to better differentiate between the ring-open and ring-closed end-products by first removing contributions to the diffraction signals originating from bromine dissociation. This study demonstrates that the cyclopropyl ring remains closed in the main dissociation channel and that the reaction products are formed promptly in less than 270 fs.

II. METHODS

A. Experimental Details

This experiment was conducted using the LCLS MeV-UED apparatus located at the SLAC National Accelerator Laboratory[11,12,14] using commercially available BCP from Sigma-Aldrich. Gaseous BCP at a pressure of 2 Torr was introduced into the interaction region using a flow cell, where the gas jet crossed paths with the UV pump and electron probe beams. The UV pump pulses at 200 nm wavelength were generated through the fourth harmonic conversion of 800 nm pulses produced by a Ti:sapphire laser system. The laser beam size on the sample was $180 \times 220\ \mu m^2$ FWHM, and the pulse duration was ∼100 fs. The pulse energy was between 5 and 17 μJ at the interaction point. Electron pulses were accelerated via a radio frequency field to 3.7 MeV before reaching the interaction region, where they were diffracted by the sample BCP molecules. The resulting diffracted electrons traveled to a phosphor screen, which was imaged by an EMCCD camera using an integration time ranging from 6 to 10 s per image. The total integration time for each time delay varied from 23 to 57 min, with the longer integration times focusing on the delays near time zero. In total, ∼16.5 h of data were used in this analysis, with the experiment running at a repetition rate of 120 Hz. Using a motorized stage, the UV pump path length was varied to adjust the difference in the time of arrival of the pump and probe beams from approximately −3.5 to 9.5 ps.

B. Theory

All complete active space self-consistent field (CASSCF) and complete active space second-order perturbation (CASPT2) calculations were carried out in the OPENMOLCAS (v19.11)[23,24] electronic structure package.

The primary CASSCF active space (Fig. 2) used to model BCP comprised twelve electrons distributed over ten orbitals, six of A' symmetry and four of A'' symmetry, including the C–C and C–Br σ/σ^* orbitals and the Br-centered n orbitals. State averaging was carried out over the three and four lowest-energy singlet and triplet states, respectively, with equal weighting being given to all states within a given spin multiplicity. These calculations are denoted SA(3|4)-CASSCF(12,10) hereafter.

A secondary, smaller CASSCF active space (Fig. 3; using the cyclopropyl radical as an exemplar) with the C–Br σ/σ^* and Br-centered n orbitals omitted was used to model the dissociation products and comprised seven electrons distributed over seven orbitals, four of A' symmetry and three of A'' symmetry, with no state averaging. These calculations are denoted CASSCF(7,7) hereafter.

CASPT2 calculations were carried out on top of the SA(3|4)-CASSCF(12,10) calculations to validate the results. Ionization

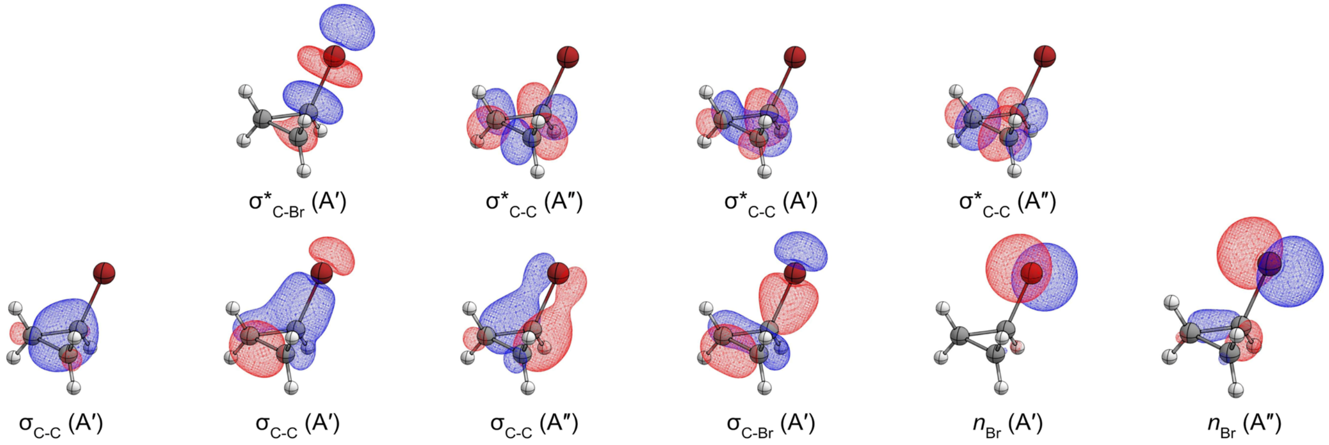

FIG. 2. BCP CASSCF active space, comprising four σ orbitals, two n orbitals, and four σ* orbitals. In total, twelve electrons were distributed over ten orbitals [CASSCF(12,10)].

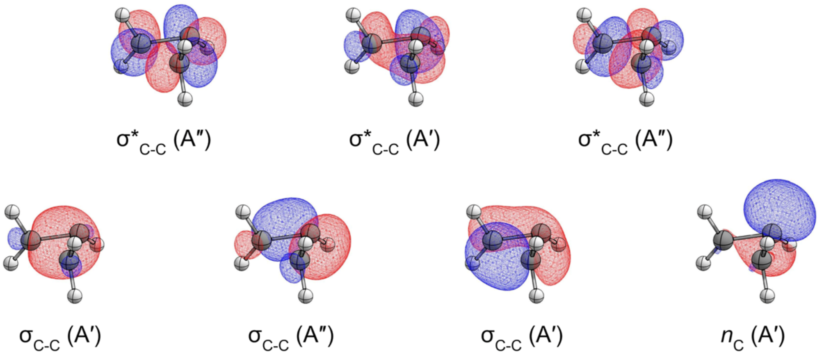

FIG. 3. BCP dissociation product CASSCF active space, comprising three σ orbitals, one n orbital, and three σ* orbitals. A total of seven electrons were distributed over seven orbitals [CASSCF(7,7)].

potential/electron affinity (IPEA) and imaginary shifts relative to the zeroth-order Hamiltonian of 0.25 and 0.1 a.u., respectively, were used. These calculations are denoted CASPT2(12,10) hereafter. The def2-SV(P) basis set was used throughout.[25]

Trajectory surface-hopping dynamics (TSHD) simulations were performed at the SA(3|4)-CASSCF(12,10)/def2-SV(P) level using the SHARC (v2.1)[26,27] TSHD wrapper interfaced with the OPENMOLCAS (v19.11)[23,24] electronic structure package. The 3 and 4 lowest-energy singlet and triplet states, respectively, were all active and coupled in the TSHD simulations through the SHARC approach for arbitrary couplings.[27–29] All energies and gradients were scaled by a constant factor of 0.925, obtained by fitting the SA(3|4)-CASSCF(12,10)/def2-SV(P) potential energy surface along the dissociation coordinate to that calculated at the (higher) CASPT2(12,10)/def2-SV(P) level. Each geometry in a Wigner-distributed ensemble of 500 independent S_0-state starting geometries was projected onto the S_1 state, and 200 independent excited-state trajectories were recorded by propagating the 200 initial conditions with the highest oscillator strength for the excitation through time for 1 ps. The nuclei were propagated via the integration of Newton's classical equations in time steps of 0.5 fs using the velocity-Verlet algorithm, while the time-dependent Schrödinger equation was integrated in time steps of 0.025 fs using the fourth-order Runge–Kutta algorithm. The TSHD decoherence parameter was set to 0.1 a.u.[30] It has been suggested that in BCP[6] and iodocyclopropane,[8] ring-opening may occur by first forming an ion-pair state consisting of a cyclopropyl cation and a bromine/iodine anion. The resulting cyclopropyl cation more easily undergoes ring-opening, yielding an allyl cation and a bromine/iodine anion, which then transitions back to a valence state. The active space used in this work is able to simulate this ion-pair state as one of the possible pathways to the ring-open product. The trajectory simulations suggest that excitation to Rydberg states is not occurring. While the CASSCF/CASPT2 active space does not include the orbitals necessary to represent the Rydberg states, the current active space is very stable, showing no signs of instabilities that may point to the presence of Rydberg states.

III. RESULTS AND DISCUSSION

We begin by examining the time-independent electron diffraction patterns collected without laser excitation to confirm that the pattern obtained from experimental measurements of gas-phase BCP agrees with theoretical calculations for the computed ground-state structure. The results of our analysis (shown in Fig. 4) indicate good agreement with the theory in both the reciprocal space (*sM*)

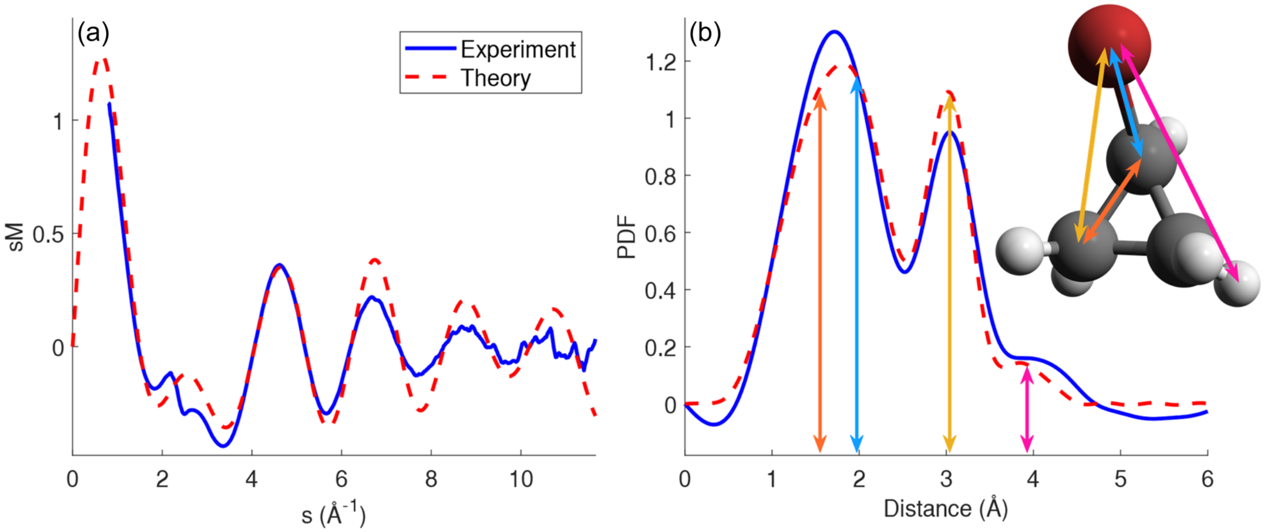

FIG. 4. (a) Static BCP sM experimental signal compared with the theoretically calculated signal of BCP molecules taken from TSHD simulations at time zero. (b) Experimental and theoretical PDF signals showing the atom pair distances present in the BCP molecular geometry. Several key atom pair distances in BCP are marked with arrows showing the distances that contribute to each of the peaks observed in the PDF signal.

signal and the real space pair distribution function (PDF). Here, *s* is the momentum transfer in units of Å^{-1}. Details on calculating these signals can be found in the supplementary material. Some of the atom pair distances in BCP are marked on the PDF. The first broad peak in the PDF (~1.8 Å) corresponds to the C–C (~1.5 Å) and C–Br (~2.0 Å) bond distances, while the nonbonded C–Br (~3.0 Å) distances give rise to the second peak in the PDF (~3.0 Å). A small peak corresponding to the longest nonbonded H–Br distances can also be seen in the PDF (~3.9 Å). All shorter bonded and nonbonded (e.g., H–C and H–Br) distances overlap with the more prominent features and are subsumed, making them difficult to observe.

Figure 5(a) shows the experimental time-dependent normalized diffraction difference intensity (ΔI/I). The ΔI/I is the normalized difference between the diffraction signal after laser excitation and the diffraction signal before laser excitation and is calculated according to Eq. (S5) of the supplementary material, Sec. 1. We first examine the signal time dependence by integrating the ΔI/I over the region $1.38 < s < 1.96$ Å^{-1} corresponding to the first positive feature in Fig. 5(a). A rise time of 270 ± 120 fs FWHM is retrieved by fitting an error function to the experimental signal. We note that this timescale is slower than the predicted rise time derived from our theoretical simulations (<100 fs). We attribute this difference to the limited time resolution of our experiment. While experiments using this instrument have achieved time resolutions down to ~150 fs,[11] we observed timing drifts during the long acquisition times that could have affected the instrument response function. Figure 5(c) shows the time-dependence of the ΔI/I calculated using molecular structures from the TSHD simulations, while Fig. 5(d) shows the same theoretical signal after convolution with a 270-fs-FWHM Gaussian kernel modeling the instrument response function. The smoothed theoretical signal, shown in Fig. 5(d), shows good agreement with the experiment in terms of peak locations, while the fast oscillations observed in the short times in Fig. 5(c) are not captured due to the finite time resolution, as can also be seen in Fig. 5(d). These oscillations are mostly due to the fast increase in the distance between the two fragments after dissociation. The observed signal reflects the appearance of the end-products present after the conclusion of the reaction. The constant shape and amplitude of the signal after a few hundred femtoseconds indicate that the final products are formed on the femtosecond timescale. The following analysis focuses on determining the branching ratio of these end-products using the data collected after 500 fs as the experimental signal strength has plateaued by this time.

The experimental ΔI/I is fit to a combination of the signals from ring-open and ring-closed end-products in order to determine the branching ratio of this reaction. Assuming that only these two end-products are produced, this fitting is performed by minimizing the chi-squared value,

$$\chi^2 = \sum_{s=1.14}^{11.66} \frac{|Signal_{\exp}(s) - E \times [p \times Signal_{Closed}(s) + (1-p) \times Signal_{Open}(s)]|^2}{\sigma(s)^2}, \tag{1}$$

where, for time delays sufficiently far after time zero such that the signal is no longer changing with time, E is the proportion of molecules excited by the laser, p is the proportion of the excited BCP molecules that produce the ring-closed product (pathway A), and σ is the uncertainty in the experimental signal. For this fit, the *Signal*(s) functions correspond to the ΔI/I. The signal uncertainty is determined via bootstrapping of the data as described in Sec. 2 of the supplementary material. We have carried out the fitting using two different sets of fitting bases. One basis is constructed from the TSHD simulations, while the other uses hot end-product simulated structures. The first fitting basis is constructed from the TSHD simulations, in which all trajectories result in bromine dissociation, with 199 trajectories yielding ring-closed end-products (pathway A), while the remaining one trajectory produces a ring-open end-product (pathway B), giving a theoretical branching ratio of 99.5% ring-closed, 0.5% ring-open. The ring-closed basis signal is calculated by averaging the ΔI/I for each geometry in the 199 ring-closed trajectories from 500 to 1000 fs. Within the single observed ring-opening trajectory, the C–Br bond dissociation and ring-opening occur sequentially, with the bromine atom

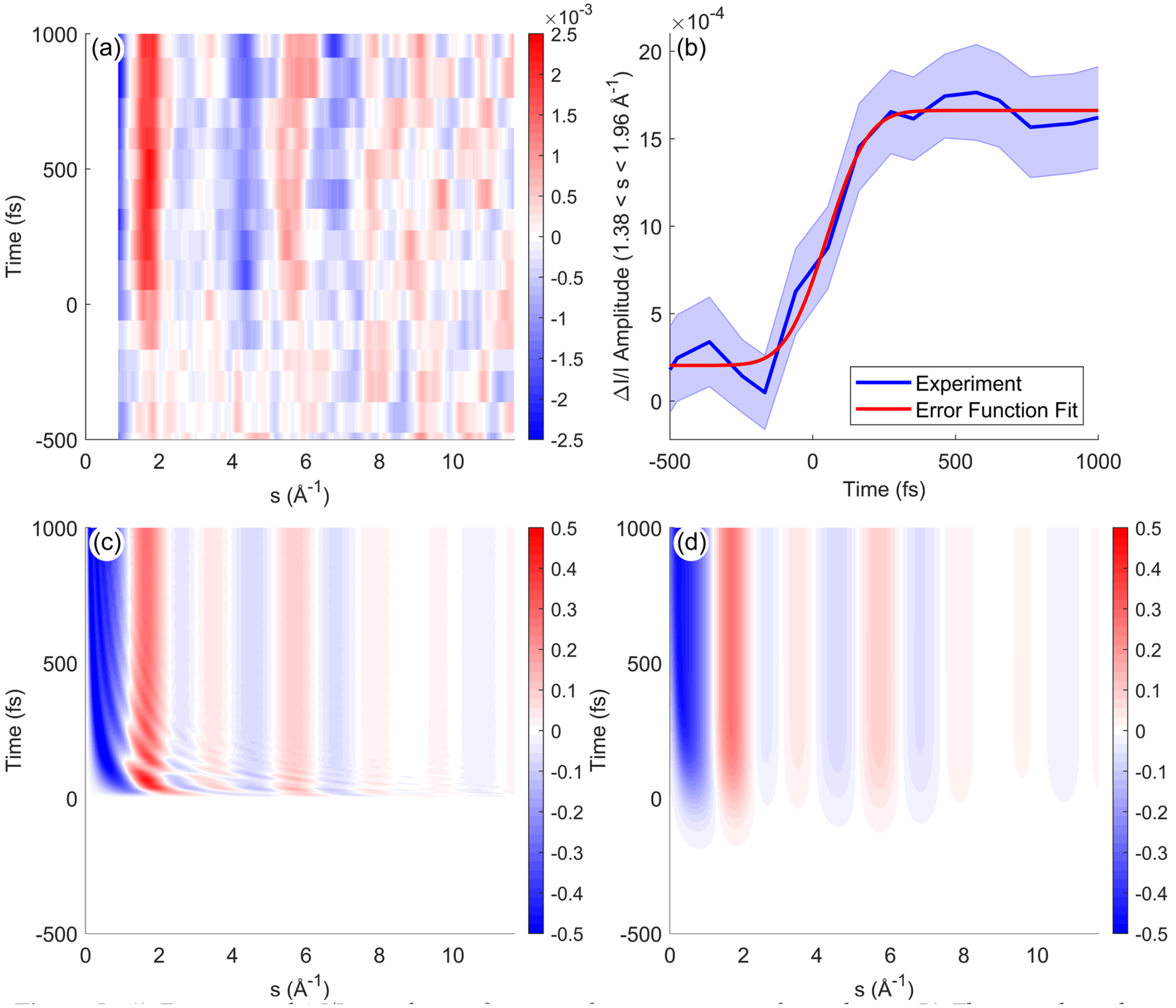

FIG. 5. (a) Experimental ΔI/I signal as a function of momentum transfer and time. (b) Time-dependent amplitude of the experimental ΔI/I signal from $1.38 < s < 1.96$ Å^{-1}. Fitting the rise of this feature with an error function gives a relatively long rise time of 270 ± 120 fs FWHM. This slow rise is attributed to the time resolution of the experiment, likely due to timing drifts during data collection. (c) Simulated ΔI/I signal from 200 BCP trajectories given a time resolution of 0.5 fs. Near time zero, the dynamics of the bromine dissociation and resulting changes in the cyclopropyl ring can be seen. (d) Simulated ΔI/I signal given in (c) smoothed with a Gaussian kernel of width 270 fs FWHM in time and 0.2 Å^{-1} FWHM in momentum transfer to reproduce the experiment resolution. After smoothing, the experimental and theoretical signals show good agreement. The early time dynamics are no longer visible due to the experiment resolution.

dissociating near time zero, while the ring remains closed until ~800 fs after time zero, meaning that only 381 individual ring-open structures are available from the TSHD simulations. The ring-open basis signal is calculated by averaging the ΔI/I for the geometries in the one ring-open trajectory from 810 to 1000 fs. The ΔI/I signals before 500 fs are excluded from the end-product fitting basis to avoid any dynamics present near time zero, while the sampled time range for the ring-open trajectory is limited to only the times after the completion of the ring-opening dynamics. The fitting is performed over the momentum transfer range $1.14 < s < 11.66$ Å^{-1}. The resulting experimental branching ratio is 86% ± 15% ring-closed (pathway A) and 14% ± 15% ring-open (pathway B), with an excitation ratio $E = 0.7\% \pm 0.1\%$. The fit results agree reasonably well with the theoretical predictions from our TSHD simulations within the uncertainties, confirming the ring-closed cyclopropyl radical product as the main channel. The experimental results, however, do predict a larger proportion of ring-opening than was predicted by simulation.

A second fitting basis has been constructed using the average ΔI/I signal from 10 000 ring-open (allyl radical) and 10 000 ring-closed (cyclopropyl radical) hot end-product simulated structures. This second basis was considered, as the previously mentioned trajectory basis contains only a single ring-open trajectory with 381 structures, which may not be representative of all possible ring-open geometries. The ring-open basis function calculated from these hot end-product structures should resolve this possible issue with the first (TSHD) basis set. Using this hot end-product basis, the resulting branching ratio is 86% ± 15% ring-closed (pathway A) and 14% ± 15% ring-open (pathway B) with an excitation ratio $E = 0.7\% \pm 0.1\%$, which is consistent with the results from the first fitting method. While the two sets of basis functions give the same branching ratios, the hot end-product basis is used in the remaining analysis due to the limited number of theoretical ring-open geometries available from the TSHD simulations. Figure 6(a) shows the experimental ΔI/I averaged over all times from 0.5 to 9.5 ps along with the total theoretical signal comprising the sum of the two basis functions weighted according to the branching ratio fit results. The two basis functions used during the fitting procedure are also plotted for comparison. The two basis functions are quite similar over the range of the experimental measurement, which is what causes the large uncertainties in the fits. The reason for the similarity is the bromine dissociation, which produces a difference signal that is significantly larger than that produced by the opening of the ring. Figure 6(b) depicts the real space ΔPDF experimental and theory signals showing the atom pair distances, which disappear during photodissociation. Both the ΔI/I and ΔPDF experiment signals agree well with the theoretical signals created using the ΔI/I branching ratio fit.

We now introduce a new fitting method to enhance the differences between the ring-closed and ring-opened dissociation product signals and produce basis functions that are more easily differentiated. In the previous fitting method, the basis functions are quite similar since the majority of the ΔI/I and ΔPDF signals come from the photodissociation of the bromine atom (bromine has a much larger scattering amplitude than carbon and hydrogen since the atomic scattering amplitude scales approximately linearly with atomic number). In this new fitting method, we first subtract the contribution to the difference signal from the bromine atom dissociation using a theoretical calculation of the ΔI/I or ΔPDF that would be produced by bromine dissociation without any other structural changes. What remains after the subtraction shows stronger differences depending on whether the ring remains closed or opens. The following formulas are used to construct these new double-differential signals, or ΔΔI/I and ΔΔPDF:

$$\frac{\Delta\Delta I}{I}(s) = \frac{\Delta I}{I}(s) - E \times \frac{\Delta I}{I}(s)_{BrDissociation}, \tag{2}$$

$$\Delta\Delta PDF(r) = \Delta PDF(r) - E \times \Delta PDF(r)_{BrDissociation}. \tag{3}$$

The bromine dissociation signal is calculated using the theoretical S_0-state BCP structure with the bromine atom removed and without otherwise altering the remaining geometry. The excitation ratio, E, is determined from the fitting results using Eq. (1) on either the ΔI/I or ΔPDF signal (with fitting performed from $0 < r < 5$ Å). Using Eqs. (2) and (3), the double-differential signals are calculated

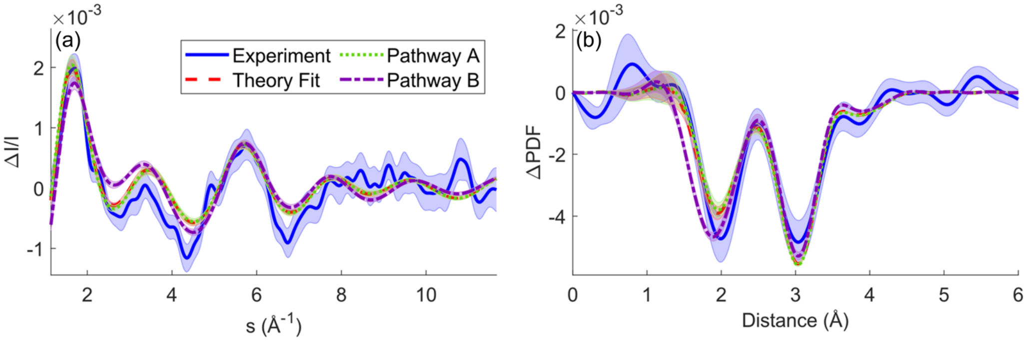

FIG. 6. (a) Lineout of the experimental ΔI/I signal after 500 fs compared to the theoretical signal. This theoretical signal is created using the branching ratio determined during the fitting using the hot end-product fitting basis. Also shown are the two basis functions used during the fit. The shaded region of the experimental signal represents the standard deviation of the signal determined via bootstrapping. The shaded regions of the theory signals represent the standard deviations of the signals determined from the 10 000 simulated structures for each of the two end-products. (b) Lineout of the experimental ΔPDF signal after 500 fs compared to the theoretical signal created using the branching ratio determined by the ΔI/I fit. Also shown is the hot end-product fitting basis. Both the ΔI/I and ΔPDF theory signals agree well with the experiment.

for both the experimental signal and theoretical hot end-product geometries. For the theoretical data, *E* is taken to be one since all simulated molecules are excited. A comparison between the differential and double-differential fitting basis functions is shown in Fig. 7. Both the ΔΔI/I and ΔΔPDF show enhanced contrast between the ring-open and ring-closed basis functions when compared to the previously used differential bases. The ΔΔPDF [Fig. 7(d)] in particular allows the two reaction pathways to be easily distinguished based on the contrast between the two basis functions near 1.5 Å. The large valley in the pathway B signal around this distance corresponds to the loss of one of the C–C bonded distances during the opening of the cyclopropyl ring. The peak near 2.7 Å in ΔΔPDF signals of both pathways can be explained by the leftward shift of the negative peak near 3 Å in the bromine dissociation ΔPDF when compared to the ΔPDF of pathways A and B, which results in a positive feature in the ΔΔPDF after the bromine dissociation signal is subtracted. The relative shift in the ΔPDF peak locations arises from differences in the reference scattering signals (the diffraction signals before laser excitation) used during their calculations. For the ring-open and ring-closed basis functions (pathways A and B), the reference scattering signal is computed from the trajectory simulation geometries at t = 0 fs. However, for the bromine dissociation signal, the reference signal is computed from the theoretically calculated S_0-state BCP structure. The atom pair distances present in these two references are slightly different, leading to the relative shift in the peak locations of the ΔPDF.

After constructing this new basis, fitting on the ΔΔI/I has been carried out according to Eq. (1) to determine the reaction branching ratio. Lineouts of these double-differential signals using all data collected from 0.5 to 9.5 ps are shown in Fig. 8.

Figure 8(a) shows the experimental ΔΔI/I, the basis functions, and the best fit signal. With this method, the experimental data clearly match the ring-closed (pathway A) structure more closely. In particular, the ring-closed signal has much better agreement with the experiment around the region from 1 to 3 $Å^{-1}$. Performing the end-product fit on this signal returns a branching ratio of 88% ± 11% ring-closed (pathway A) and 12% ± 11% ring-open (pathway B). The real space ΔΔPDF signal is also investigated since the unique atom pair distances present in the ring-open and ring-closed geometries allow a more obvious differentiation between these two reaction pathways. This analysis, pictured in Fig. 8(b), shows that the ring-closed signal follows the experimental signal more closely, agreeing with the ΔΔI/I result. This is especially obvious in the ΔΔPDF signal near 1.4–1.9 Å, where the ring-open signal deviates quite far from the experiment, while the ring-closed signal matches more closely. While the ΔΔPDF comparison offers a qualitative confirmation of

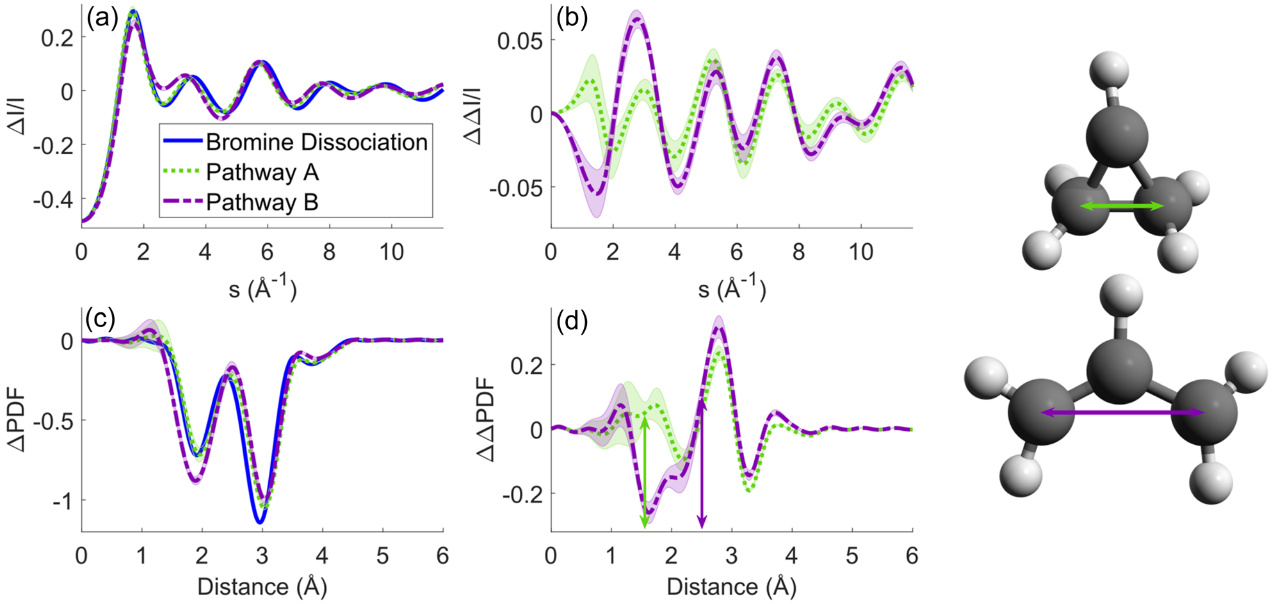

FIG. 7. (a) ΔI/I signal of bromine dissociation (blue solid line) from the optimized ground state BCP geometry compared with the hot end-product fitting basis signals (pathway A: green dashed line; pathway B: purple dashed line). Both hot end-product signals resemble the signal from bromine dissociation, making the differentiation between the ring-closed and ring-open end-products difficult. The shaded regions of each signal represent the standard deviations determined from the 10 000 simulated hot end-product structures. The bromine dissociation signal's standard deviation is zero as it is calculated from a single structure. (b) ΔΔI/I hot end-product signals calculated by subtracting the bromine dissociation signal from the hot end-product ΔI/I. These signals show greater contrast with one another, especially at $s < 4$ $Å^{-1}$, allowing more accurate end-product fitting. (c) ΔPDF signals of bromine dissociation compared with the hot end-product signals. Just as in the ΔI/I, the two hot end-product signals resemble the bromine dissociation signal, as the loss of the bromine atom dominates the signal. (d) ΔΔPDF signals of the hot end-products. These signals are easily distinguishable near 2 Å due to the increase in one of the three C–C distances as the ring opens. The green and purple vertical arrows represent the mean C–C distance, which opens during the ring-opening reaction calculated using the hot end-product structures. (Right) A hot end-product ring-closed and ring-open molecule showing the C–C distance, which lengthens as the ring opens.

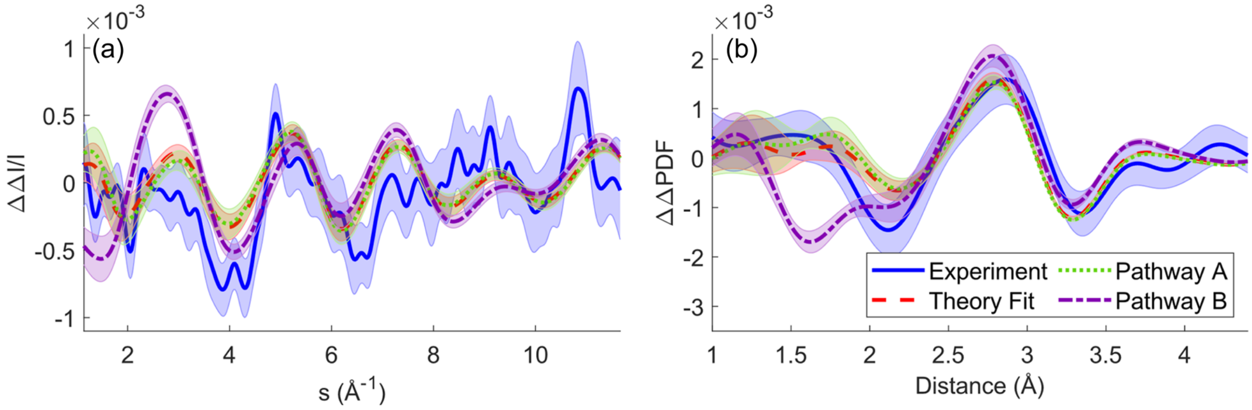

FIG. 8. (a) Lineout of the experimental ΔΔI/I signal compared to the theoretical signal from the ring-open and ring-closed hot end-products, as well as a line of best fit combining the theoretical signals using the branching ratio determined from the fit. (b) Lineout of the experimental ΔΔPDF signal compared to the theoretical signal from the ring-open and ring-closed hot end-products, as well as the signal constructed from the branching ratio fit of the ΔΔI/I signal. Both the ΔΔI/I and ΔΔPDF signals more easily differentiate between the ring-open and ring-closed signals when compared to our previous fitting basis with the ring-closed signal agreeing more closely with the experiment.

our fit, it contains more theoretical input than the momentum space ΔΔI/I signal. This dependence on the theory arises from the missing signal in the diffraction images at low s values, which is filled by the hot end-product computed signal for $s < 1.38$ Å^{-1} using the ΔI/I fit branching ratio. We, therefore, defer the quantitative branching ratio fit to the ΔΔI/I. The results from the double-differential fitting method are fully consistent with the previous (standard) method. However, this new method reduces the uncertainties by a factor of ∼1.3, from 15 to 11%. Removal of the strong dissociation signature, which is present in both reaction channels, allows the subtle differences in the signals to be more easily differentiated, reducing the uncertainty in the branching ratio fit. This improvement is further highlighted in Fig. 9, which compares the shape of the χ^2 curves for the ΔI/I and ΔΔI/I hot end-product bases as a function of the reaction branching ratio computed using Eq. (1). The χ^2 curves have been normalized such that the minimum values of each curve are one for easier comparison between the two fitting results. Comparing the results of the two fitting bases, it is clear that the double-differential fitting basis results in a steeper χ^2 dependence on the branching ratio with a better-defined minimum. This comparison indicates that the double-differential fitting basis is more easily able to differentiate between the two end-products, giving a smaller uncertainty in the resulting branching ratio. We expect that this double differential method can also be applied to other diffraction experiments, where dissociation or another large signal obscures the differences between the end-products of different channels.

Comparing our results to previous experiments, the analysis by Pandit *et al.* of velocity-map imaging results[6] with nanosecond resolution inferred from their total kinetic energy release data that fewer than 5% of excited BCP molecules yield the ring-open end-product after bromine dissociation when excited at 230–267 nm. Using UED, which is directly sensitive to changes in the molecular geometry, our experimental results predict a higher yield of 12% ± 11% ring-open structures, although 5% is within the measurement uncertainty. From Pandit *et al.*,[6] the reaction enthalpy of the C–Br bond dissociation was calculated to be 337.9 kJ mol^{-1}, while

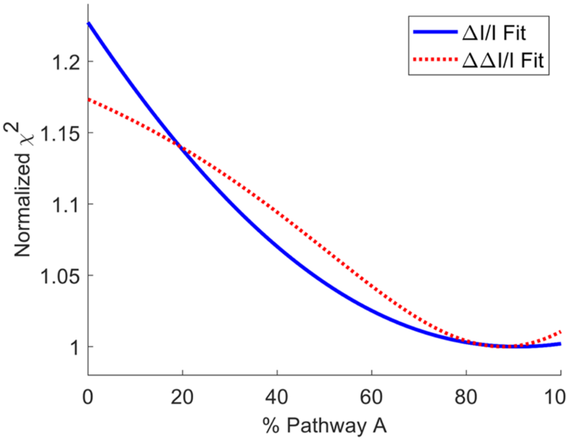

FIG. 9. χ^2 values computed using Eq. (1) for all reaction branching ratios for both the ΔI/I and ΔΔI/I hot end-product bases. The two plotted curves represent the average χ^2 value at each branching ratio across all the bootstrapped datasets. The χ^2 values have been scaled such that the minimum value of each curve is one.

the average of the total kinetic energy release distribution of the Br + cyclopropyl ring bond cleavage at 230 nm was centered near 100 kJ mol^{-1} (see Fig. 4 of Pandit *et al.*).[6] Subtracting the bond dissociation energy and average total kinetic energy release from the photon energies of 230 and 200 nm gives an estimated internal energy for the cyclopropyl radical of ∼80 kJ mol^{-1} and ∼160 kJ mol^{-1}, respectively. The estimated activation energy for the ring-opening of the cyclopropyl radical has been found to be 80–92 kJ mol^{-1}.[6,8,31–33] While the total kinetic energy release distribution will depend on the photon energy, these approximate calculations suggest that the ring-open product should in fact be more favorable in this 200 nm experiment when compared to Pandit *et al.* and that the ring-opening should eventually occur for most excited molecules in our experiment. Examining our TSHD calculations, the majority of the simulated cyclopropyl fragments have internal energies >100 kJ mol^{-1}, meaning that they should eventually isomerize to ring-open allyl fragments. However, only one of our 200 trajectories completes this isomerization within the 1 ps timeframe spanned by our simulations. Together, our estimation of the cyclopropyl fragment internal energy after excitation with 200 nm, along with our experimental and TSHD simulation results, suggests that the C–Br dissociation and cyclopropyl ring-opening processes predominantly occur sequentially, not in a concerted fashion. While the breaking of the C–Br bond occurs on an ultrafast (<1 ps) timescale, the ring-opening process appears to occur over a much longer timescale (>>1 ps) as a barrier-crossing must occur to form the ring-open allyl product. Together, the results of the VMI experiment from Pandit *et al.* and this UED experiment suggest that the yield of ring-opened dissociation products is likely greater than predicted by our theory.

In previous work, Arnold *et al.* suggested that for iodocyclopropane,[8] ring-opening may occur by first forming an ion-pair state in which ring-opening can more easily occur. Pandit *et al.* suggested that this pathway may also contribute to ring-opening in BCP.[6] This process would require a seam of conical intersections between the valence and ion-pair states to allow the excited molecules to move between these two electronic states. We were not able to locate the reported conical intersections for BCP or iodocyclopropane using a higher level of theory [CASSCF(12,10)/def2-SV(P)] than that used in Arnold *et al.*[8] and were also unable to reproduce the results of Arnold *et al.*[8] and locate the reported conical intersection for iodocyclopropane at the CASSCF(4,4) level employed in that work. From Arnold *et al.*,[8] the purported ion-pair ring-opening pathway requires the iodine atom to remain in the vicinity of the cyclopropyl fragment during the ring-opening process. Both our TSHD simulations and UED experimental results instead suggest that bromine atom dissociation occurs much more quickly than the ring-opening of the cyclopropyl radical, with the two processes happening in a sequential, not concerted manner. We, therefore, see no evidence of this ion-pair state playing a role in the creation of the ring-open products observed in this experiment.

IV. CONCLUSIONS

Based on our analysis of the UED data, we conclude that the ring-closed cyclopropyl radical dissociation product is the dominant channel in the 200 nm wavelength photodissociation of gaseous BCP and that the dissociation products form in less than 270 fs. The branching ratio between ring-closed cyclopropyl radicals and the minority ring-opened allyl radical products of C–Br bond cleavage was verified using three fitting approaches, including a new double-differential method to enhance the differences between the UED signals used as fitting basis functions for ring-closed and ring-opened products. This method removes the contribution from the C–Br bond dissociation, which produces a strong signal that is present for both channels and obscures the differences between the end-products in the diffraction signal. Our results are consistent with previous velocity-map imaging experimental results[6] and our theoretical TSHD simulations, suggesting that, while the majority of excited BCP molecules yield cyclopropyl radicals after bromine-atom dissociation, concerted ring-opening and C–Br bond fission is likely a minor reaction pathway. However, our experimental measurements suggest that the yield of ring-opened dissociation products may be greater than predicted by theory. The double-differential technique used here could also be applicable to other photodissociation UED experiments, allowing more precise differentiation of two or more similar end-products.

SUPPLEMENTARY MATERIAL

The following information can be found in the supplementary material: Sec. I. Diffraction theory: An overview of the theory used in the analysis of electron diffraction data. Sec. II. Data processing and additional analysis steps: An explanation of the steps taken to process the raw diffraction images into the signals used in the data analysis.

ACKNOWLEDGMENTS

MeV-UED is operated as part of the Linac Coherent Light Source at the SLAC National Accelerator Laboratory, supported by the U.S. Department of Energy, Office of Science, Office of Basic Energy Sciences, under Contract No. DE-AC02-76SF00515. We acknowledge support from the Atomic, Molecular, and Optical Sciences Program of the U.S. Department of Energy, Office of Science, Office of Basic Energy Sciences, Chemical Sciences, Geosciences, and Biosciences Division under Award Nos. DE-SC0014170 (J.L., C.L., S.K.S., K.J.W., Y.X., and M.C.) and DE-AC02-76SF00515 (M.W. and T.J.A.W.). A.J.O.E. acknowledges EPSRC for support from Program Grant No. EP/V026690/1. X.W. acknowledges support by the Deutsche Forschungsgemeinschaft (DFG, German Research Foundation) through the Collaborative Research Centre (CRC) 1242 (Project No. 278162697, Project C01 Structural Dynamics in Impulsively Excited Nanostructures) and funding by the DFG Germany's Excellence Strategy – EXC 2033 – 390677874 – RESOLV.

AUTHOR DECLARATIONS

Conflict of Interest

The authors have no conflicts to disclose.

Author Contributions

Jackson Lederer: Formal analysis (lead); Software (supporting); Visualization (lead); Writing – original draft (lead); Writing – review & editing (equal). **J. Pedro F. Nunes**: Conceptualization (lead); Formal analysis (supporting); Investigation (equal); Software (supporting); Writing – review & editing (equal). **Conor D. Rankine**: Formal analysis (supporting); Investigation (equal); Software (lead); Visualization (supporting); Writing – original draft (supporting); Writing – review & editing (equal). **Andrew R. Attar**: Investigation (equal). **Kareem Hegazy**: Investigation (equal). **Fuhao Ji**: Investigation (equal). **Cuong Le**: Formal analysis (supporting); Software (supporting). **Ming-Fu Lin**: Investigation (equal). **Yusong Liu**: Investigation (equal); Writing – review & editing (equal). **Duan Luo**: Investigation (equal). **Andrew J. Orr-Ewing**: Formal analysis (supporting); Writing – review & editing (equal). **Sajib Kumar Saha**: Investigation (equal). **Xiaozhe Shen**: Investigation (equal). **Xijie Wang**: Investigation (equal). **Matthew Ware**: Investigation (equal). **Stephen P. Weathersby**: Investigation (equal). **Kyle J. Wilkin**: Investigation (equal). **Thomas J. A. Wolf**: Investigation (equal). **Yanwei Xiong**: Investigation (equal). **Jie Yang**: Investigation (equal). **Martin Centurion**: Formal analysis (supporting); Funding acquisition (lead); Investigation (equal); Supervision (lead); Writing – review & editing (equal).

DATA AVAILABILITY

The data that support the findings of this study are openly available in Zenodo at https://doi.org/10.5281/zenodo.16414639.

REFERENCES

[1] S. C. Wofsy, M. B. McElroy, and Y. L. Yung, "The chemistry of atmospheric bromine," Geophys. Res. Lett. **2**(6), 215–218, https://doi.org/10.1029/gl002i006p00215 (1975).

[2] W. R. Simpson, R. von Glasow, K. Riedel, P. Anderson, P. Ariya, J. Bottenheim, J. Burrows, L. J. Carpenter, U. Frieß, M. E. Goodsite, D. Heard, M. Hutterli, H.-W. Jacobi, L. Kaleschke, B. Neff, J. Plane, U. Platt, A. Richter, H. Roscoe, R. Sander, P. Shepson, J. Sodeau, A. Steffen, T. Wagner, and E. Wolff, "Halogens and their role in polar boundary-layer ozone depletion," Atmos. Chem. Phys. **7**(16), 4375–4418 (2007).

[3] J. S. Daniel, S. Solomon, R. W. Portmann, and R. R. Garcia, "Stratospheric ozone destruction: The importance of bromine relative to chlorine," J. Geophys. Res.: Atmos. **104**(D19), 23871–23880, https://doi.org/10.1029/1999jd900381 (1999).

[4] B.-M. Sinnhuber, N. Sheode, M. Sinnhuber, M. P. Chipperfield, and W. Feng, "The contribution of anthropogenic bromine emissions to past stratospheric ozone trends: A modelling study," Atmos. Chem. Phys. **9**(8), 2863–2871 (2009).

[5] S. Ohnishi, M. Murata, and S. Kawanishi, "DNA damage induced by hypochlorite and hypobromite with reference to inflammation-associated carcinogenesis," Cancer Lett. **178**(1), 37–42 (2002).

[6] S. Pandit, T. J. Preston, S. J. King, C. Vallance, and A. J. Orr-Ewing, "Evidence for concerted ring opening and C–Br bond breaking in UV-excited bromocyclopropane," J. Chem. Phys. **144**(24), 244312 (2016).

[7] X. Zheng, C. W. Lee, and D. L. Phillips, "Resonance Raman observation of the allyl cation produced after ultraviolet photodissociation of cyclopropyl bromide in acetonitrile solution," Chem. Phys. Lett. **366**(5–6), 656–663 (2002).

[8] P. A. Arnold, B. R. Cosofret, S. M. Dylewski, P. L. Houston, and B. K. Carpenter, "Evidence of a double surface crossing between open- and closed-shell surfaces in the photodissociation of Cyclopropyl iodide," J. Phys. Chem. A **105**(10), 1693–1701 (2001).

[9] C. J. Marsden, L. Hedberg, and K. Hedberg, "Molecular structure of bromocyclopropane by gas electron diffraction with use of rotational constants and by ab initio calculation," J. Phys. Chem. **92**(7), 1766–1770 (1988).

[10] M. Centurion, T. J. A. Wolf, and J. Yang, "Ultrafast imaging of molecules with electron diffraction," Annu. Rev. Phys. Chem. **73**, 21–42 (2022).

[11] X. Shen, J. P. F. Nunes, J. Yang, R. K. Jobe, R. K. Li, M.-F. Lin, B. Moore, M. Niebuhr, S. P. Weathersby, T. J. A. Wolf, C. Yoneda, M. Guehr, M. Centurion, and X. J. Wang, "Femtosecond gas-phase mega-electron-volt ultrafast electron diffraction," Struct. Dyn. **6**(5), 054305 (2019).

[12] S. P. Weathersby, G. Brown, M. Centurion, T. F. Chase, R. Coffee, J. Corbett, J. P. Eichner, J. C. Frisch, A. R. Fry, M. Gühr, N. Hartmann, C. Hast, R. Hettel, R. K. Jobe, E. N. Jongewaard, J. R. Lewandowski, R. K. Li, A. M. Lindenberg, I. Makasyuk, J. E. May, D. McCormick, M. N. Nguyen, A. H. Reid, X. Shen, K. Sokolowski-Tinten, T. Vecchione, S. L. Vetter, J. Wu, J. Yang, H. A. Dürr, and X. J. Wang, "Mega-electron-volt ultrafast electron diffraction at SLAC national accelerator laboratory," Rev. Sci. Instrum. **86**(7), 073702 (2015).

[13] J. Yang, M. Guehr, X. Shen, R. Li, T. Vecchione, R. Coffee, J. Corbett, A. Fry, N. Hartmann, C. Hast, K. Hegazy, K. Jobe, I. Makasyuk, J. Robinson, M. S. Robinson, S. Vetter, S. Weathersby, C. Yoneda, X. Wang, and M. Centurion, "Diffractive imaging of coherent nuclear motion in isolated molecules," Phys. Rev. Lett. **117**(15), 153002 (2016).

[14] J. Yang, M. Guehr, T. Vecchione, M. S. Robinson, R. Li, N. Hartmann, X. Shen, R. Coffee, J. Corbett, A. Fry, K. Gaffney, T. Gorkhover, C. Hast, K. Jobe, I. Makasyuk, A. Reid, J. Robinson, S. Vetter, F. Wang, S. Weathersby, C. Yoneda, X. Wang, and M. Centurion, "Femtosecond gas phase electron diffraction with MeV electrons," Faraday Discuss. **194**, 563–581 (2016).

[15] J. Yang, X. Zhu, T. J. A. Wolf, Z. Li, J. P. F. Nunes, R. Coffee, J. P. Cryan, M. Gühr, K. Hegazy, T. F. Heinz, K. Jobe, R. Li, X. Shen, T. Veccione, S. Weathersby, K. J. Wilkin, C. Yoneda, Q. Zheng, T. J. Martinez, M. Centurion, and X. Wang, "Imaging CF_3 I conical intersection and photodissociation dynamics with ultrafast electron diffraction," Science **361**(6397), 64–67 (2018).

[16] Y. Liu, S. L. Horton, J. Yang, J. P. F. Nunes, X. Shen, T. J. A. Wolf, R. Forbes, C. Cheng, B. Moore, M. Centurion, K. Hegazy, R. Li, M.-F. Lin, A. Stolow, P. Hockett, T. Rozgonyi, P. Marquetand, X. Wang, and T. Weinacht, "Spectroscopic and structural probing of excited-state molecular dynamics with time-resolved photoelectron spectroscopy and ultrafast electron diffraction," Phys. Rev. X **10**(2), 021016 (2020).

[17] K. J. Wilkin, R. M. Parrish, J. Yang, T. J. A. Wolf, J. P. F. Nunes, M. Guehr, R. Li, X. Shen, Q. Zheng, X. Wang, T. J. Martinez, and M. Centurion, "Diffractive imaging of dissociation and ground-state dynamics in a complex molecule," Phys. Rev. A **100**(2), 023402 (2019).

[18] T. Wang, H. Jiang, C. Jin, X. Zou, P. Zhu, T. Jiang, F. He, and D. Xiang, "Imaging the photochemical dynamics of cyclobutanone with MeV ultrafast electron diffraction," J. Chem. Phys. **162**(18), 184201 (2025).

[19] A. E. Green, Y. Liu, F. Allum, M. Graßl, P. Lenzen, M. N. R. Ashfold, S. Bhattacharyya, X. Cheng, M. Centurion, S. W. Crane, R. Forbes, N. A. Goff, L. Huang, B. Kaufman, M.-F. Kling, P. L. Kramer, H. V. S. Lam, K. A. Larsen, R. Lemons, M.-F. Lin, A. J. Orr-Ewing, D. Rolles, A. Rudenko, S. K. Saha, J. Searles, X. Shen, S. Weathersby, P. M. Weber, H. Zhao, and T. J. A. Wolf, "Imaging the photochemistry of cyclobutanone using ultrafast electron diffraction: Experimental results," J. Chem. Phys. **162**(18), 184303 (2025).

[20] E. G. Champenois, D. M. Sanchez, J. Yang, J. P. Figueira Nunes, A. Attar, M. Centurion, R. Forbes, M. Gühr, K. Hegazy, F. Ji, S. K. Saha, Y. Liu, M.-F. Lin, D. Luo, B. Moore, X. Shen, M. R. Ware, X. J. Wang, T. J. Martínez, and T. J. A. Wolf, "Conformer-specific photochemistry imaged in real space and time," Science **374**(6564), 178–182 (2021).

[21] T. J. A. Wolf, D. M. Sanchez, J. Yang, R. M. Parrish, J. P. F. Nunes, M. Centurion, R. Coffee, J. P. Cryan, M. Gühr, K. Hegazy, A. Kirrander, R. K. Li, J. Ruddock, X. Shen, T. Vecchione, S. P. Weathersby, P. M. Weber, K. Wilkin, H. Yong, Q. Zheng, X. J. Wang, M. P. Minitti, and T. J. Martínez, "The photochemical ring-opening of 1,3-cyclohexadiene imaged by ultrafast electron diffraction," Nat. Chem. **11**(6), 504–509 (2019).

[22] R. S. Mulliken, "Intensities in molecular electronic spectra X. Calculations on mixed-halogen, hydrogen halide, alkyl halide, and hydroxyl spectra," J. Chem. Phys. **8**(5), 382–395 (1940).

[23] I. Fdez Galván, M. Vacher, A. Alavi, C. Angeli, F. Aquilante, J. Autschbach, J. J. Bao, S. I. Bokarev, N. A. Bogdanov, R. K. Carlson, L. F. Chibotaru, J. Creutzberg, N. Dattani, M. G. Delcey, S. S. Dong, A. Dreuw, L. Freitag, L. M. Frutos, L. Gagliardi, F. Gendron, A. Giussani, L. González, G. Grell, M. Guo, C. E. Hoyer, M. Johansson, S. Keller, S. Knecht, G. Kovačević, E. Källman, G. Li Manni, M. Lundberg, Y. Ma, S. Mai, J. P. Malhado, P. Å. Malmqvist, P. Marquetand, S. A. Mewes, J. Norell, M. Olivucci, M. Oppel, Q. M. Phung, K. Pierloot, F. Plasser, M. Reiher, A. M. Sand, I. Schapiro, P. Sharma, C. J. Stein, L. K. Sørensen, D. G. Truhlar, M. Ugandi, L. Ungur, A. Valentini, S. Vancoillie, V. Veryazov, O. Weser, T. A. Wesołowski, P.-O. Widmark, S. Wouters, A. Zech, J. P. Zobel, and R. Lindh, "OpenMolcas: From source code to insight," J. Chem. Theory Comput. **15**(11), 5925–5964 (2019).

[24] F. Aquilante, J. Autschbach, A. Baiardi, S. Battaglia, V. A. Borin, L. F. Chibotaru, I. Conti, L. De Vico, M. Delcey, I. Fdez Galván, N. Ferré, L. Freitag, M. Garavelli, X. Gong, S. Knecht, E. D. Larsson, R. Lindh, M. Lundberg, P. Å. Malmqvist, A. Nenov, J. Norell, M. Odelius, M. Olivucci, T. B. Pedersen, L. Pedraza-González, Q. M. Phung, K. Pierloot, M. Reiher, I. Schapiro, J. Segarra-Martí, F. Segatta, L. Seijo, S. Sen, D.-C. Sergentu, C. J. Stein, L. Ungur, M. Vacher, A. Valentini, and V. Veryazov, "Modern quantum chemistry with [open]Molcas," J. Chem. Phys. **152**(21), 214117 (2020).

[25] F. Weigend and R. Ahlrichs, "Balanced basis sets of split valence, triple zeta valence and quadruple zeta valence quality for H to Rn: Design and assessment of accuracy," Phys. Chem. Chem. Phys. **7**(18), 3297 (2005).

[26] S. Mai, D. Avagliano, M. Heindl, P. Marquetand, M. F. S. J. Menger, M. Oppel, F. Plasser, S. Polonius, M. Ruckenbauer, Y. Shu, D. G. Truhlar, L. Zhang, P. Zobel, and L. González (2023). "SHARC: Surface hopping including arbitrary couplings–Program package for non-adiabatic dynamics," GitHub. https://doi.org/10.5281/zenodo.7828641

[27] S. Mai, P. Marquetand, and L. González, "Nonadiabatic dynamics: The SHARC approach," WIREs Comput. Mol. Sci. **8**(6), e1370 (2018).

[28] M. Richter, P. Marquetand, J. González-Vázquez, I. Sola, and L. González, "SHARC: *Ab initio* molecular dynamics with surface hopping in the adiabatic representation including arbitrary couplings," J. Chem. Theory Comput. **7**(5), 1253–1258 (2011).

[29] S. Mai, P. Marquetand, and L. González, "A general method to describe intersystem crossing dynamics in trajectory surface hopping," Int. J. Quantum Chem. **115**(18), 1215–1231 (2015).

[30] G. Granucci and M. Persico, "Critical appraisal of the fewest switches algorithm for surface hopping," J. Chem. Phys. **126**(13), 134114 (2007).

[31] G. Greig and J. C. J. Thynne, "Reactions of cyclic alkyl radicals. Part 1.—Methyl-radical-sensitized decomposition of cyclopropane carboxyldehyde," Trans. Faraday Soc. **62**, 3338–3344 (1966).

[32] G. Greig and J. C. J. Thynne, "Reactions of cyclic alkyl radicals. Part 2.—Photolysis of cyclopropane carboxaldehyde," Trans. Faraday Soc. **63**, 1369–1374 (1967).

[33] J. A. Kerr, A. Smith, and A. F. Trotman-Dickenson, "Reactions of cyclopropyl radicals in the methyl-initiated decomposition of cyclopropanecarbaldehyde," J. Chem. Soc. A **1969**, 1400–1403.